Practical method to estimate parameters of elasto-plastic constitutive model for unsaturated soils from compaction curve

Tachibana, Shinya
Matsumoto, Masayoshi
Iizuka, Atsushi

(Citation)
Soils and Foundations,60(5):1287-1298

(Issue Date)
2020-10

(Resource Type)
journal article

(Version)
Version of Record

(URL)
https://hdl.handle.net/20.500.14094/90007726

HOSTED BY
ELSEVIER
Available online at www.sciencedirect.com
ScienceDirect
Soils and Foundations 60 (2020) 1287–1298
SOILS AND FOUNDATIONS
www.elsevier.com/locate/sandf

Technical Paper

Practical method to estimate parameters of elasto-plastic constitutive model for unsaturated soils from compaction curve

Shinya Tachibana [a,*], Masayoshi Matsumoto [b], Atsushi Iizuka [a]

[a] *Research Center for Urban Safety and Security, Kobe University, Japan*
[b] *Hyogo Prefectural Government (formerly, Graduate School of Engineering Faculty of Engineering, Kobe University), Japan*

Received 31 July 2019; received in revised form 4 May 2020; accepted 13 August 2020
Available online 24 September 2020

Abstract

The input parameters for the hardening law for the elasto-plastic constitutive model of unsaturated soils are generally fitting parameters that control the degree of hardening response and cannot easily be determined without the results of experimental tests in which the changes in suction, water content, and volume are measured or controlled. However, it is next to impossible to complete such precise experimental tests on all the geomaterials comprising the earth structure to be analysed, such as an embankment. It is important, therefore, to establish a method for determining these parameters from more easily attainable data on the material. This paper presents a practical method for estimating the input parameters related to hardening/softening due to desaturation/saturation in the elasto-plastic constitutive model proposed by Ohno et al. (2007a) from a compaction curve, which is frequently obtained and widely used in engineering practice. In the proposed method, the input parameters are estimated by simultaneously solving three theoretical equations, each of which holds for a different point, indicating the statically compacted state on the dry side of the compaction curve, while the approximately represented compaction curve is used instead of a hand-drawn one. The paper demonstrates that the proposed method enables the estimation of the input parameter values within a range small enough so as not to affect the results of the simulation, irrespective of the way in which the points on the represented compaction curve are selected. The validity of the estimated parameters is verified and then discussed through a series of static compaction test simulations.

Keywords: Unsaturated soils; Compaction curve; Elasto-plastic constitutive equation; Hardening law

1. Introduction

Since Bishop (1960) proposed an effective stress formula for unsaturated soils, great advancements have been made in unsaturated soil mechanics. In particular, various constitutive models for unsaturated soils have been proposed since the pioneering work of Alonso et al. (1990). The constitutive modelling for unsaturated soils has been reviewed in state-of-the-art reports, as exemplified by Gens (1996), Wheeler and Karube (1996), Kohgo (2003), Gens et al. (2008), Sheng and Fredlund (2008), Sheng et al. (2008), and Cui and Sun (2009). In many elasto-plastic constitutive models, the hardening law for the unsaturated elasto-plastic constitutive model associated with desaturation is expressed as a function of the degree of saturation and/or suction. Ohno et al. (2007a) proposed an elasto-plastic constitutive model (called the 'Se-Hardening model') to express the expansion and contraction of a yield surface by stipulating the elastic region in the arbitrary unsaturated state and introducing the effective degree of saturation as a

Peer review under responsibility of The Japanese Geotechnical Society.
* Corresponding author.
E-mail address: stachi@people.kobe-u.ac.jp (S. Tachibana).

https://doi.org/10.1016/j.sandf.2020.08.005
0038-0806/

variable. The Se-hardening model assumes that the normal compression lines of the constant degree of saturation are parallel to each other in the $e - \ln p'$ space, in which e is the void ratio and p' is the effective mean stress, and require two fitting parameters to determine the degree of translation of the normal compression line along the axis of the effective mean stress with changes in the degree of saturation, as will be explained in more detail in the following section. Conversely, several normal compression lines, differing in their degrees of saturation, need to be identified through a series of compression tests on the material for which the parameters are determined. However, this is not easy because, in principle, the degree of saturation cannot be kept constant during the tests. According to Ohno et al. (2007a), the isograms of the degree of saturation were drawn in the $e - \ln p'$ space based on several normal compression lines for the constant water content, which is nothing more than an attempt to identify the normal compression curved surface in the $e - \ln p' - S_r$ space. Although Lloret-Cabot et al. (2017) also fitted the normal compression planar surface in the $v - \ln p^* - \ln s^*$ space, in which v is the specific volume, p^* is the mean Bishop's stress, and s^* is the modified suction, to determine the material inputs for their Glasgow coupled model formulated by Lloret-Cabot et al. (2014), it seems that the results of compression tests under at least three different conditions were necessary.

It is indeed straightforward and essential to determine the input parameters of the constitutive model to be employed in the analysis with higher reliability through minute experiments accompanied by the control or measurement of the changes in suction, water content, and volume. Meanwhile, the fact remains that an alternative approach to determining them from more easily available data should be of value for engineering practice, particularly if it is difficult to complete such tests. From this viewpoint, a practical method is herein proposed to estimate the two fitting parameters controlling the hardening law of the Se-hardening model from three sets of values for the water content and dry density on the compaction curve that is widely used in engineering practice.

This paper is organised as follows. In Section 2, after giving an overview of the Se-hardening model, a theoretical equation is formulated for the statically compacted state based on some assumptions and a method is explained in which the input parameters are estimated by simultaneously solving three equations for three points on the compaction curve. Then, in Section 3, the dry side of the compaction curve is approximately represented and parameterized using a ternary phase diagram in order to deal with it as a continuous function and to allow the arbitrary selection of three points even from a limited range. In Section 4, the input parameters are estimated for silty clay using the proposed method. Finally, in Section 5, the validity of the estimated parameters is verified through simulations of static compaction tests.

2. Estimation method for input parameters related to hardening law

The hardening law for the elasto-plastic constitutive model by Ohno et al. (2007a) is formulated as a function of effective degree of saturation S_e defined as

$$S_e = \frac{S_r - S_{r0}}{1 - S_{r0}} \tag{1}$$

in which S_r is the degree of saturation and subscript 0 denotes the value at the driest state where only meniscus water around the soil particle remains. The effective degree of saturation is related to suction and water retention, specifying the unsaturated state of the soil.

The effective stress for the unsaturated state employed in the model is defined as follows:

$$\boldsymbol{\sigma}' = \boldsymbol{\sigma}^{net} + S_e s \mathbf{1} \tag{2}$$

where $\boldsymbol{\sigma}'$ is the effective stress tensor, $\boldsymbol{\sigma}^{net}$ is the net stress tensor, s is suction, and $\mathbf{1}$ is the identity tensor of the order two. Then, the yield function of the model is expressed as

$$f\left(\boldsymbol{\sigma}', \varepsilon_v^p, S_e\right) = \frac{\lambda - \kappa}{1 + e_0} \ln \frac{p'}{\xi p'_{sat0}} + \frac{\lambda - \kappa}{1 + e_0} \frac{1}{n_E} \left(\frac{\eta}{M}\right)^{n_E} - \varepsilon_v^p = 0 \tag{3}$$

where λ is the compression index, κ is the swelling index, M is the critical state parameter introduced in the Cam-clay model, p' is the effective mean stress, p'_{sat0} is the pre-consolidation pressure under the fully saturated condition, e is the void ratio, e_0 is the void ratio at the reference, ε_v^p is the plastic component of volumetric strain, $\eta = q/p'$ is the stress ratio, and n_E is a parameter applied to adjust the rate of dilatancy development, as introduced by Ohno et al. (2007b, 2013). The yield surface can expand/shrink not only due to the development of plastic volumetric strain, but also due to changes in the effective degree of saturation. Thus, the size of the yield surface or pre-consolidation pressure p'_c at the unsaturated state is expressed as

$$p'_c = \xi p'_{sat}; \; p'_{sat} = p'_{sat0} \exp \frac{\varepsilon_v^p}{(\lambda - \kappa)/(1 + e_0)} \tag{4}$$

and

$$\xi = \xi(S_e) = \exp[(1 - S_e)^n \ln a] \tag{5}$$

where variable ξ determines the degree of the effect of desaturation on the pre-consolidation pressure, and n and a are the material parameters used to control the degree of softening/hardening behaviour with saturation/desaturation. The schematic expression for the hardening associated with saturation and desaturation is shown in Fig. 1. The yield surface maintains its shape and passes the origin of the effective stress space at any state, as shown in Fig. 1 (a), which implies that the shear strength always becomes zero at zero effective mean stress regardless of the magnitude of the effective degree of saturation. Fig. 1(b) shows a conceptual chart of the transition of the normal compres-

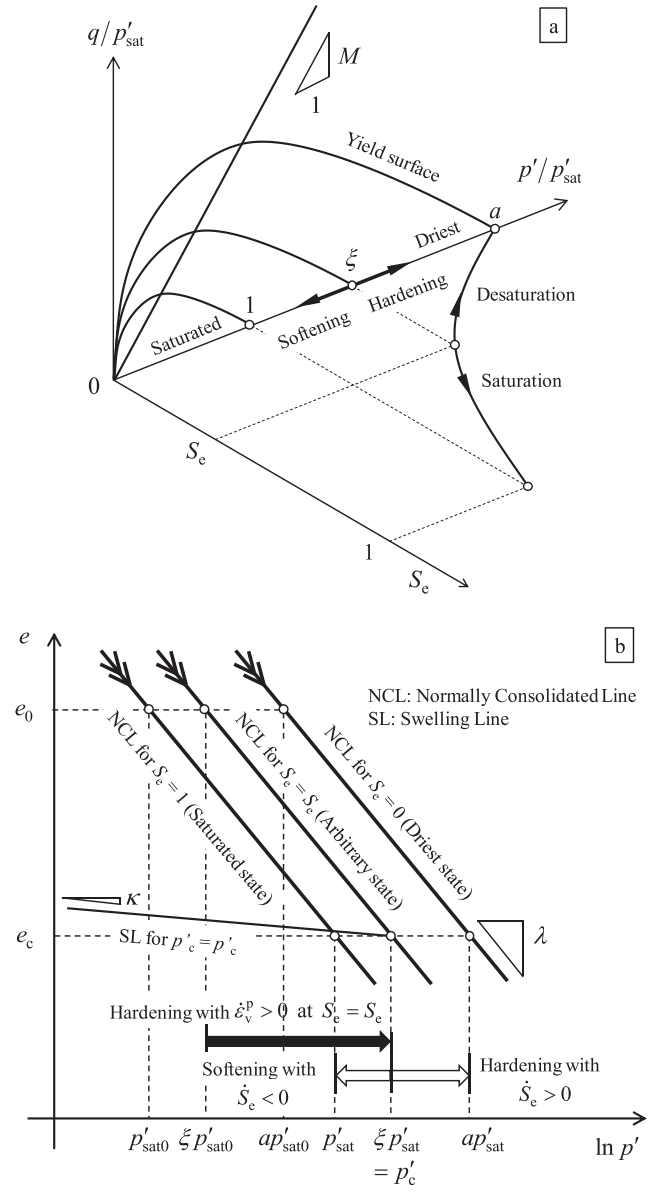

Fig. 1. Hardening behavior in Se-hardening model in (a) p'-q- S_e space and (b) e-lnp' space (Ohno et al., 2007a).

sion line (NCL) due to changes in the effective degree of saturation. The constitutive model employed in this study assumes that compression index λ, which is a slope of the NCL in the $e - \ln p'$ space, remains unchanged irrespective of the variation in the effective degrees of saturation, although some different expressions have been proposed in previous researches. Alonso et al. (1990), Kohgo et al. (1993), and Zhou et al. (2012), for example, each proposed a constitutive model in which the compression index was formulated as a function of suction so that it would decrease with desaturation. Conversely, in Wheeler and Sivakumar (1995) and Loret and Khalili (2002), the compression index was formulated such that it would increase with desaturation. Although the existence of such a variety of models is a reminder that there may be an adequate expression for compressibility, depending on the material or the stress range to be analysed, the present paper does not address this issue in depth.

The estimation method for these two parameters, n and a, shall basically be tailored for use with the compaction curve obtained from the static compaction tests on an object material for which the stress history is definite. For this purpose, the following assumptions and simplifications are made: 1) The undrained condition for pore water always holds during static compaction, which implies no change in the water content; 2) No excess pore air pressure is generated in the specimen owing to the fully drained condition for pore air; 3) During compaction, the stress condition of the specimen remains isotropic; 4) The compacted state on the compaction curve is considered to be in a stress-free state when the specimen has been unloaded monotonically and elastically from the elasto-plastic state where the maximum confining stress was applied; 5) The change in void ratio during unloading is negligible because it is sufficiently small compared to that observed during elasto-plastic loading; 6) The soil-water retention characteristic curve is assumed to be given uniquely, and thus, the hysteresis loop between the drying and wetting processes is not considered.

Now, as shown in Fig. 2, three points,$\alpha = 1, 2, 3$, are chosen on the compaction curve obtained from the static compaction tests in which the same maximum confining stress p_{max} was applied as in the past. Herein, the combination of water content w and dry density ρ_d at point α is represented by w_α and $\rho_{d,\alpha}$. Then, we have

$$e_\alpha = \frac{\rho_w}{\rho_{d,\alpha}} G_s - 1 \tag{6}$$

$$S_{r,\alpha} = \frac{w_\alpha G_s}{e_\alpha} \tag{7}$$

and

$$S_{e,\alpha} = \frac{S_{r,\alpha} - S_{r0}}{1 - S_{r0}} \tag{8}$$

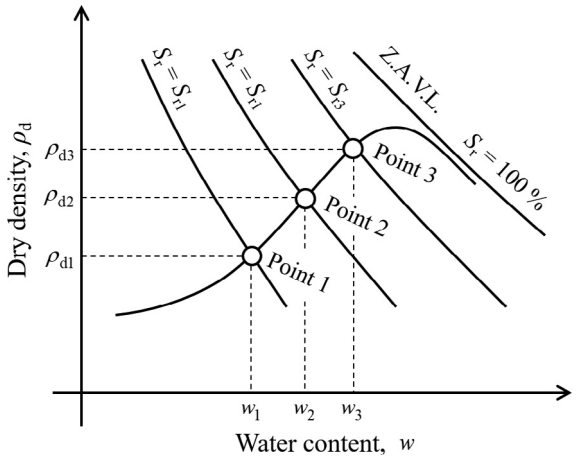

Fig. 2. Sampling points on compaction curve.

where ρ_w is the density of the pore water and G_s is the specific gravity of the soil particles. Symbols e_α, $S_{r,\alpha}$, and $S_{e,\alpha}$ indicate the void ratio, degree of saturation, effective degree of saturation at point α, respectively.

As for Assumption 6), the soil-water characteristic curve employed in this paper shows a one-to-one relationship between suction and the degree of saturation, after Sugii and Uno (1995), in the following form:

$$\frac{S_r - S_{ra}}{S_{rf} - S_{ra}} = \frac{1}{1 + \exp(A + B\ln s)} \tag{9}$$

where S_{rf} is the degree of saturation at $s = 0$, S_{ra} is the degree of residual saturation at $s \to \infty$, and A and B are constant parameters. In this paper, it is assumed that $S_{rf} = 1.0$ and $S_{ra} = S_{r0}$; and thus, the left-hand side of Eq. (9) becomes equal to effective degree of saturation S_e. Then, the suction at point α, denoted by s_α, is uniquely determined against $S_{e,\alpha}$ from the inverse relationship given in Eq. (9) as

$$s_\alpha = \exp\left[\frac{1}{B}\left(-A + \ln\frac{1 - S_{e,\alpha}}{S_{e,\alpha}}\right)\right] (\alpha = 1, 2, 3) \tag{10}$$

From Assumption 3), the stress state of a specimen can be represented by the isotropic stresses as

$$\boldsymbol{\sigma}' = p'\mathbf{1} = (p^{net} + S_e s)\mathbf{1} \tag{11}$$

where p^{net} is the mean net stress which always corresponds to the mean total stress, i.e., $p^{net} = p$ based on Assumption 2). Since the state at point α on the compaction curve is stress-free ($p = 0$), the effective mean stress at point α, denoted by p'_α, can be expressed by Eq. (11) as

$$p'_\alpha = S_{e,\alpha} s_\alpha (\alpha = 1, 2, 3) \tag{12}$$

Next, the past state is considered for each point α to which maximum confining stress p_{max} was applied. It is noted that the variables at that state shall be represented with an overline to distinguish them from those being unloaded, i.e., $e = \bar{e}_\alpha$ for the void ratio. Assumptions 1) and 5) allow any changes in the water content or the void ratio during unloading ($\bar{w}_\alpha = w_\alpha$ and $\bar{e}_\alpha = e_\alpha$) to be ignored, which implies that there is no change in the degree of saturation between the two states. As the effective degree of saturation and suction are uniquely determined against the degree of saturation, based on Assumption 6), the following relationships are obtained:

$$\bar{S}_{r,\alpha} = S_{r,\alpha}, \bar{S}_{e,\alpha} = S_{e,\alpha} \text{ and } \bar{s}_\alpha = s_\alpha \ (\alpha = 1, 2, 3), \tag{13}$$

Thus, by substituting Eq. (13) into Eq. (11), the effective mean stress at that past state can be expressed as

$$\bar{p}'_\alpha = \bar{p} + \bar{S}_{e,\alpha}\bar{s}_\alpha = p_{max} + S_{e,\alpha} s_\alpha \ (\alpha = 1, 2, 3) \tag{14}$$

because the total mean stress is equal to the applied maximum confining stress ($\bar{p} = p_{max}$) with Assumption 3).

Fig. 3 plots both states before and after unloading on the $e - \ln p'$ plane, corresponding to point α on the compaction curve. In this figure, two normal compression lines

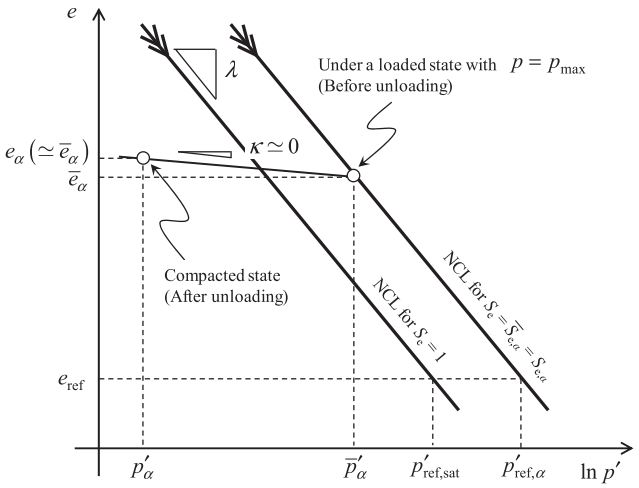

Fig. 3. Idealization of state change in unloading process.

are also drawn: one is the NCL for $S_e = S_{e,\alpha}$ against each point α, while the other is the common NCL for $S_e = 1$ against all points α. Since the state before unloading is elasto-plastic on the NCL for $S_e = S_{e,\alpha}$, based on Assumption 4), the following relationship is obtained:

$$p'_{ref,\alpha} = \bar{p}'_\alpha \exp\frac{\bar{e}_\alpha - e_{ref}}{\lambda};\ \bar{e}_\alpha = e_\alpha \ (\alpha = 1, 2, 3) \tag{15}$$

where $p'_{ref,\alpha}$ is the effective mean stress corresponding to the reference void ratio e_{ref} on the NCL when $S_e = S_{e,\alpha}$. On the other hand, since function ξ in Eq. (4) indicates the magnification of the elastic region in the elasto-plastic unsaturated state, the value of ξ for $S_e = S_{e,\alpha}$ yields

$$\xi_\alpha = \frac{p'_{ref,\alpha}}{p'_{ref,sat}} \ (\alpha = 1, 2, 3) \tag{16}$$

where ξ_α is the value of ξ for $S_e = S_{e,\alpha}$ and $p'_{ref,sat}$ is the effective mean stress corresponding to reference void ratio e_{ref} on the NCL when $S_e = 1$. On the other hand, by the definition of function ξ in Eq. (5), ξ_α can be expressed in terms of effective degree of saturation $S_{e,\alpha}$ as

$$\xi_\alpha = \exp[(1 - S_{e,\alpha})^n \ln a] (\alpha = 1, 2, 3) \tag{17}$$

By substituting Eqs. (8) and (16) into Eq. (17), the following equations are obtained for each point α:

$$\left(\frac{1 - S_{r,\alpha}}{1 - S_{r0}}\right)^n \ln a = \ln\frac{p'_{ref,\alpha}}{p'_{ref,sat}} (\alpha = 1, 2, 3) \tag{18}$$

The reason why three equations for $\alpha = 1, 2, 3$ are required to estimate the two parameters, n and a, is that there is another unknown, $p'_{ref,sat}$, which determines the location of the NCL for a saturated state, as shown in Fig. 3.

By subtracting Eq. (18) when $\alpha = 2$ from one when $\alpha = 1$, we have

$$\frac{(1 - S_{r,1})^n - (1 - S_{r,2})^n}{(1 - S_{r0})^n} \ln a = \ln\frac{p'_{ref,1}}{p'_{ref,2}} \tag{19}$$

Similarly, by subtracting Eq. (18) when $\alpha = 3$ from one when $\alpha = 2$, we have

$$\frac{(1-S_{r,2})^n - (1-S_{r,3})^n}{(1-S_{r0})^n} \ln a = \ln \frac{p'_{ref,2}}{p'_{ref,3}} \tag{20}$$

Finally, when $a \neq 1$, the following relation can be derived from Eqs. (19) and (20):

$$\frac{(1-S_{r,1})^n - (1-S_{r,2})^n}{(1-S_{r,2})^n - (1-S_{r,3})^n} = \frac{\ln \frac{p'_{ref,1}}{p'_{ref,2}}}{\ln \frac{p'_{ref,2}}{p'_{ref,3}}} \tag{21}$$

Thus, between the two parameters to be determined, parameter n can be determined first by solving Eq. (21) together with Eqs. (14) and (15) using, for example, the Newton-Raphson method. Then, the other parameter, a, can be determined by substituting the obtained parameter n into either Eq. (19) or (20) as

$$a = \exp\left[\frac{(1-S_{r0})^n}{(1-S_{r,1})^n - (1-S_{r,2})^n} \ln \frac{p'_{ref,1}}{p'_{ref,2}}\right] \tag{22}$$

It is understood, therefore, that the two parameters required in the hardening law can be determined from the three points sampled on the compaction curve, which is premised on obtaining compression index λ in advance, estimating the value of suction s_α at the three points, and clarifying maximum confining stress p_{max} in the process of a static compaction.

3. Approximate representation and parameterization of compaction curve

The following sections are devoted to verifying the effectiveness of the above-described method. The way of selecting a set of three points on the compaction curve has been arbitrary up to now; however, it may affect the calculated values of the parameters. Thus, to evaluate this influence, the compaction curve shall firstly be approximately represented and parameterized with a ternary phase diagram to deal with it as a continuous function even for a bounded scope.

Since the soil consists of three phases, namely, the soil particles, pore water, and pore air, as schematically shown in Fig. 4, the summation of the volume ratios satisfies the following:

$$\frac{V_s}{V} + \frac{V_w}{V} + \frac{V_a}{V} = 1 \tag{23}$$

where V is the volume of soil, V_s is the volume of soil particles, V_w is the volume of pore water, and V_a is the volume of pore air. Each volume ratio for the soil particles, pore water, and pore air can be rearranged as

$$\frac{V_s}{V} = \frac{M_s}{V}\frac{V_s}{M_s} = \frac{\rho_d}{\rho_s} \tag{24}$$

$$\frac{V_w}{V} = \frac{M_w}{M_s}\frac{M_s}{V}\frac{V_w}{M_w} = w\frac{\rho_d}{\rho_w} \equiv \theta \tag{25}$$

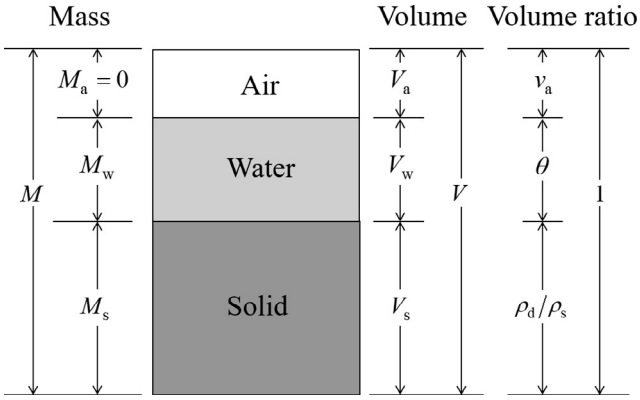

Fig. 4. Three phases and volume ratio of unsaturated soil.

$$\frac{V_a}{V} \equiv v_a \tag{26}$$

where ρ_s is the density of the soil particles, ρ_w is the density of the pore water, ρ_d is the dry density of the soil, θ is the moisture content by volume, and v_a is the pore air porosity. Therefore, Eq. (23) can be naturally replaced as follows:

$$\frac{\rho_d}{\rho_s} + \theta + v_a = 1 \tag{27}$$

It should be noted that the degree of saturation can be expressed as $S_r = \theta/(\theta + v_a)$.

According to Kobayashi (2016), the ternary phase diagram shown in Fig. 5 is of use for comprehensively representing the state of the unsaturated soil by plotting the volume ratios in Eq. (27). By setting Cartesian coordinate system $X - Y$, in which the origin coincides with the point of $v_a = 1.0$ in the ternary diagram, as in Fig. 5, the combination of the three volume ratios $(\rho_d/\rho_s, \theta, v_a)$ can be reduced to the coordinates (X, Y) as

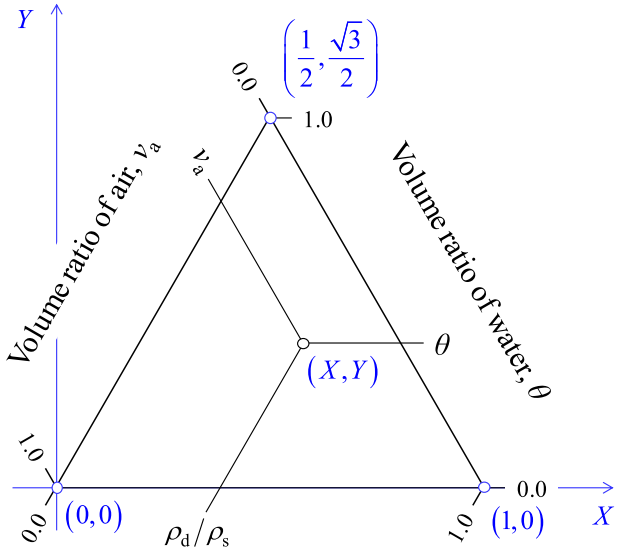

Fig. 5. Definition of ternary phase diagram.

$$X = \frac{\rho_d}{\rho_s} + \frac{1}{2}\theta \text{ and } Y = \frac{\sqrt{3}}{2}\theta \tag{28}$$

Where the points at $\rho_d/\rho_s = 1.0$, $\theta = 1.0$, and $v_a = 1.0$ correspond to coordinates $(1.0, 0.0)$, $(1/2, \sqrt{3}/2)$, and $(0.0, 0.0)$ in system $X - Y$, respectively.

The compaction curves, which are ordinally drawn on the $w - \rho_d$ plane, can be mapped on the ternary diagram. The results of compaction tests on the core material in a fill dam, reported by Mikuni (1962) and Tatsuoka (2015), and on silty clay, reported by Kawai et al. (2002), are plotted on ternary diagrams in Figs. 6 and 7, respectively. Both are the results of 'dynamic' compaction tests conducted under different energies of compaction, i.e., the number of blows per layer in a mould. It is noted that the diagrams are partially displayed to focus on the region where the experimental data exist. The compaction curves drawn on the ternary diagrams appear to have substantially the same shape, independent of the energy of compaction, but to shift along the constant line at $S_r = S_{r,opt}$, drawn by a broken line, toward the lower right hand corner, i.e., $\rho_d/\rho_s = 1.0$, with an increase in the number of blows. $S_{r,opt}$ is the optimum degree of saturation whose values can be approximately estimated as 84% for the core material in Tatsuoka (2015) and 76% for the silty clay in Kawai et al. (2002). Of particular note is that the major parts of the dry sides of the compaction curves are generally straight and almost parallel to each other in the ternary diagram. Thus, in this study, each compaction curve is expressed with its common slope β_d in Cartesian coordinate system $X - Y$, as

$$\frac{\rho_d}{\rho_s} = \left(\frac{\sqrt{3}}{2}\frac{1}{\beta_d} - \frac{1}{2}\right)\left(\theta - w^*\frac{\rho_d^*}{\rho_w}\right) + \frac{\rho_d^*}{\rho_s} \tag{29}$$

where w^* and ρ_d^* are the water content and the dry density, respectively, that correspond to the point of intersection

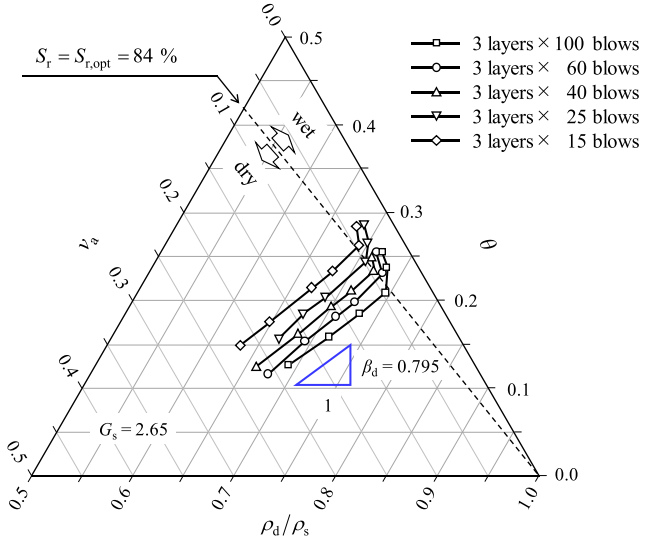

Fig. 6. Compaction curves reported by Mikuni (1962) and Tatsuoka (2015) on ternary phase diagram.

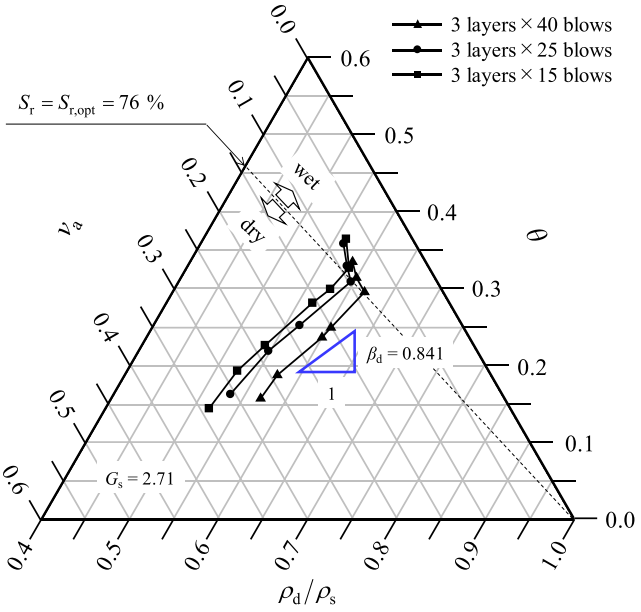

Fig. 7. Compaction curves reported by Kawai et al. (2002) on ternary phase diagram.

between the line with a slope of $\beta_d = 0.795$ and the line indicating the optimum degree of saturation, being slightly different from optimum water content w_{opt} and maximum dry density ρ_{dmax}. Eq. (29) can be rewritten as the relation between the dry density and the water content by substituting Eq. (25) into Eq. (29) as follows:

$$\rho_d = \frac{1 - k_d G_s w^*}{1 - k_d G_s w}\rho_d^*; k_d = \frac{\sqrt{3}}{2}\frac{1}{\beta_d} - \frac{1}{2} \tag{30}$$

The dry sides of each compaction curves, based on Eq. (30), are drawn by broken lines on the well-recognized $w - \rho_d$ plane in Figs. 8 and 9, each of which employs the

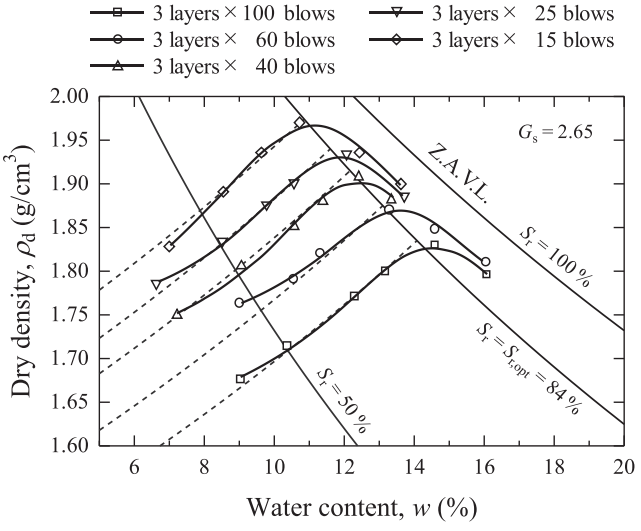

Fig. 8. Comparison between represented compaction curve (broken line) and hand-drawn compaction curve (solid line) based on data reported by Mikuni and Tatsuoka (2015).

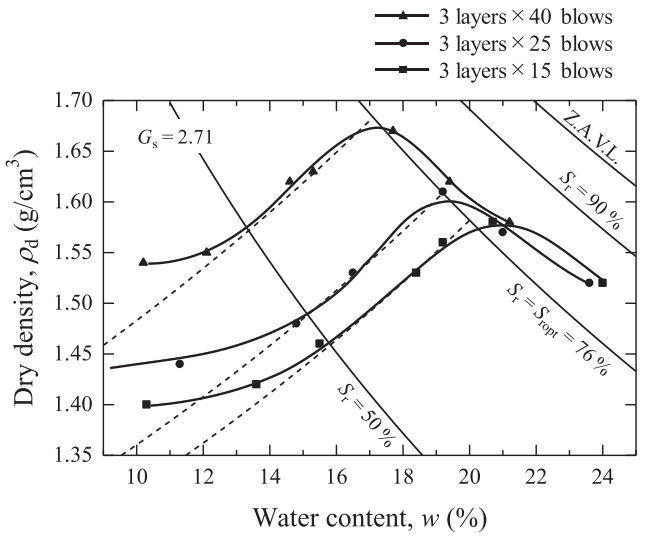

Fig. 9. Comparison between represented compaction curve (broken line) and hand-drawn compaction curve (solid line) based on data reported by Kawai et al. (2002).

Table 1
Parameters to fit dry side of compaction curves reported by Mikuni (1962) and Tatsuoka (2015).

Test condition	w^*(%)	ρ_d^*(g/cm^3)	Symbol in Figs. 6 and 8
3 layers × 100 blows	10.86	1.974	◇
3 layers × 60 blows	11.60	1.940	▽
3 layers × 40 blows	12.17	1.915	△
3 layers × 25 blows	13.10	1.875	○
3 layers × 15 blows	14.08	1.835	□

Note: $G_s = 2.65$; $S_{ropt} = 84\%$; $\beta_d = 0.795$; $k_d = 0.589$.

Table 2
Parameters to fit dry side of compaction curves reported by Kawai et al. (2002).

Test condition	w^* (%)	ρ_d^* (g/cm^3)	Symbol in Figs. 7 and 9
3 layers × 40 blows	17.10	1.683	▲
3 layers × 25 blows	19.20	1.609	●
3 layers × 10 blows	20.00	1.582	■

Note: $G_s = 2.71$; $S_{ropt} = 76\%$; $\beta_d = 0.841$; $k_d = 0.530$.

values for w^* and ρ_d^* summarised on Tables 1 and 2, respectively, for the core material in Tatsuoka (2015) and the silty clay in Kawai et al. (2002). Also drawn in these figures are the hand-drawn compaction curves with a solid line for each group of plots having the same number of blows. The curves based on Eq. (30) appear to represent the dry sides of the compaction curves at least within a range of $50\% \leqslant S_r \leqslant S_{r,opt}$ with an unique parameter β_d (or k_d) independent of the energy of compaction, once the values for w^* and ρ_d^* have been determined for each one.

4. Estimation of parameters in hardening law from compaction curve

Using the approximately represented compaction curve, the parameters required in the hardening law shall be estimated in this section. Among the 'dynamic' compaction curves represented in the preceding section, the curve for a silty clay is addressed here. This is because the estimation method is based on 'static' compaction and requires the value of the maximum confining stress to achieve the compaction curve. In fact, Kawai et al. (2002) conducted not only 'dynamic', but also 'static' compaction tests on the material; the results allow the estimation of an equivalent maximum confining stress to achieve a 'dynamic' compaction curve. Fig. 10 shows the results of both the dynamic and the static compaction tests on silty clay, in which the solid lines indicate the 'dynamic' compaction curves, appearing in the preceding section, and the contour lines represent the isograms of the maximum confining stress in a 'static' compaction to achieve the dry density against the prescribed water content. It is found from this figure that the 'dynamic' compaction curve and the isogram of the 'static' maximum confining stress are almost parallel to each other on the dry side. On the other hand,

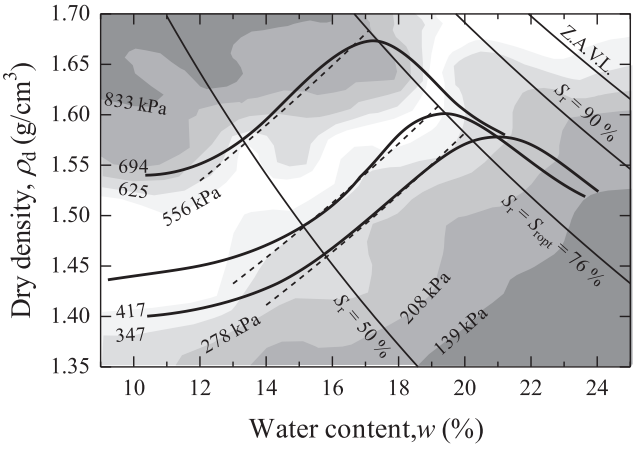

Fig. 10. Comparison between results of static and dynamic compaction tests by Kawai et al. (2002).

even on the wet side of the optimum degree of saturation, obtained from the 'static' compaction, the isogram has an upward distribution toward the zero-air void line, which suggests different mechanisms between the dynamic and static compactions on the wet side. This is the reason why only the dry side of dynamic compaction curve is formulated as Eq. (30) and is used as a source of the sampling points.

The combination of parameters n and a shall be estimated through Eqs. (21) and (22) against each set of three points on the dry side of the approximated compaction curve with the lowest compaction energy in Fig. 10. The three points are randomly chosen from a total of 100 points at equal intervals within a range of $50\% \leqslant S_r \leqslant S_{r,opt}$ where the curve based on Eq. (30) reasonably represents the compacted states, as shown in Figs. 8 and 9. Thus, the values for the degree of saturation at three points for α ($\alpha = 1, 2, 3$) are renamed as $S_{r,min}$, $S_{r,mid}$, and $S_{r,max}$ in what follows. Table 3 summarises the material properties and

loading conditions required for estimating parameters n and a. Among these values, compression index λ was determined from plasticity index $I_P = 13.2$ for silty clay by the empirical equation by Iizuka and Ohta (1987). The parameters for the soil-water characteristic curve, SWCC, were estimated using a knowledge-based database (SoilVision System Ltd., 2006). The maximum confining stress of 350 kPa was approximately estimated from the counter in Fig. 10.

The estimated values for parameters n and a are plotted against the degree of saturation at the middle point in Figs. 11 and 12, respectively. Although not all the values are plotted, it is obvious that the distribution of both values is not so wide, namely, within a range of $50\% \leqslant S_r \leqslant S_{r,opt}$, i.e., $1.257 \leqslant n \leqslant 1.773$ and $4.096 \leqslant \ln a \leqslant 4.607$. Fig. 13 shows the combination of estimated values for parameters n and a. Although an attempt was made to estimate these values, including the points on the wet side of the 'dynamic' compaction curve, the values became unrealistic or indefinite when including even one of them. According to the analytical investigation by Kanazawa et al. (2012), the compaction curve calculated as a solution to initial-boundary value problems is considerably influenced by the air permeability and the loading rate. By considering the distribution of isograms of the maximum confining stress in the static compaction together, the decrease in dry density with the increase in water content at a relatively higher degree of saturation, common in dynamic compaction, seems difficult to obtain in static compaction under a fully drained condition for pore air.

5. Validation of estimated parameters through simulations of static compaction

There is a variation, although small, between the estimated values for parameters n and a, as shown in Fig. 13. Therefore, this section examines the influence of this variation on the simulation results of static compaction. It also validates the static compaction response, including the compaction curve, obtained as the results of the simulation with the estimated parameters, by considering the initial state of compaction from the theoretical viewpoint.

Table 3
Material properties for silty clay and loading condition required to estimate parameters n and a.

Notation	Symbol	Value
Specific gravity of soil particles	G_s	2.71
Compression index	λ	0.1074*
Residual degree of saturation	S_{r0}	0.15
Parameters for SWCC	A	−18.0
	B	4.6
Maximum confining stress	p_{max}	350 kPa

* $\lambda = 0.015 + 0.007 I_P$; Plasticity index: $I_P = 13.2$.

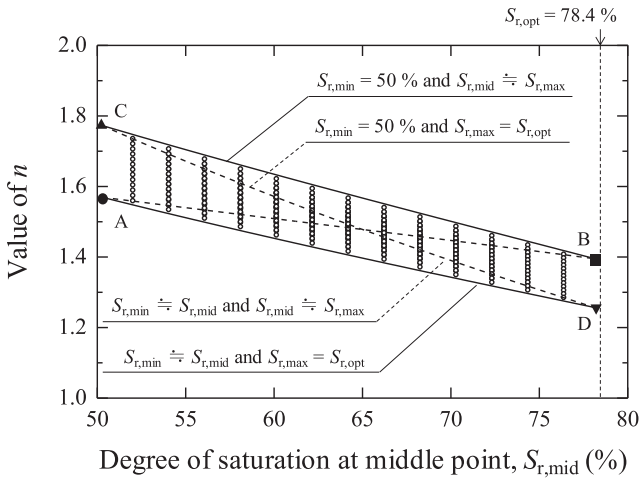

Fig. 11. Estimated values for parameter n.

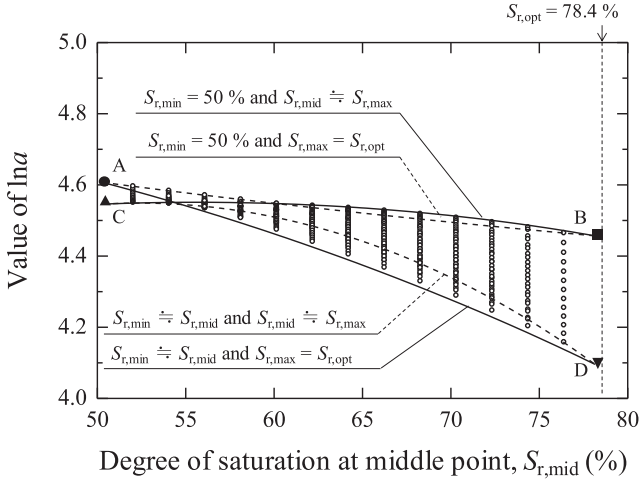

Fig. 12. Estimated values for parameter a.

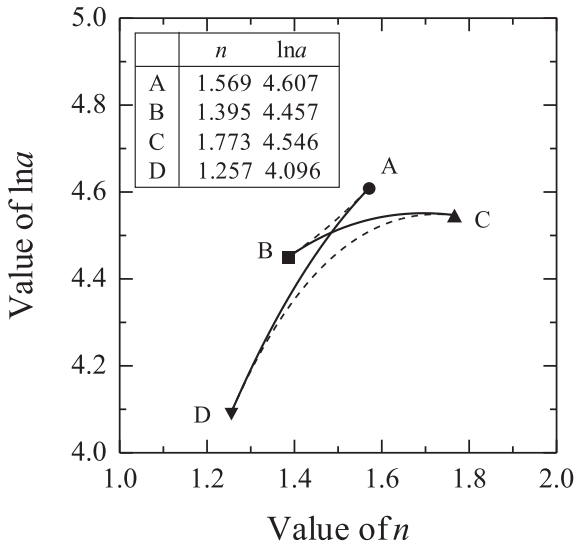

Fig. 13. Relation between estimated parameters n and a.

The simulation shall basically be carried out in conformity to the assumptions to idealise the static compaction described in Section 1. Each combination of parameters n and a for cases A to D, shown in Fig. 13, is employed in the simulation, while the other parameters are commonly used. Table 4 summarises the additional parameters not given on Table. 3. Herein, the swelling index is assumed to be significantly small ($\kappa = 0.001$). The initial void ratio before loading was also set to be 1.0 in all the calculations, since the values for the void ratio were about 1.0 at most in the early stage of the static compaction according to Kawai et al. (2002); however, the validity of this value will be discussed later.

Fig. 14 shows the results of the simulation of static compaction under the isotropic condition. Herein, the simulation of static compaction is conducted for a wider range of water contents ($10\% \leqslant w \leqslant 30\%$), although the three points required for estimating parameters n and a were chosen from the range of $50\% \leqslant S_r \leqslant S_{r,opt}$ on the dry side of the represented compaction curve. The calculated values for dry density against a set of water contents are almost independent of the combination from A to D at least within the range of $50\% \leqslant S_r \leqslant S_{r,opt}$. This suggests that the proposed method can estimate appropriate values for parameters n and a without affecting the results of the simulation independent of the method for sampling the three points. The line joining the points calculated in each case is almost parallel to the represented compaction curve, which supports the considerable accuracy of the proposed method. On the other hand, it is found that the results of the simulation have a slightly lower value for dry density even on the dry side compared with the target represented compaction curve. In fact, it is no wonder that this kind of discrepancy exists because the proposed method relies merely on the state change with a relatively small rebound from the elasto-plastic state, where the maximum confining stress is applied, to the elastically unloaded state; it does not ensure the prediction of a larger volume change due to the loading from the initial stress-free state. Although the only way to achieve a more highly accurate reproduction of the compaction curve is to modify the constitutive model, including reconsidering the hardening law, so as to cover a wider range in void ratios, it is beyond the scope of this paper.

Meanwhile, it is worth deliberating initial void ratio e_i from a theoretical viewpoint based on a few assumptions concerning the initial state before loading, although it

Table 4
Additional material parameters required for simulation of static compaction.

Notation	Symbol	Value
Swelling index	κ	0.001
Critical state parameter	M	1.34
Poisson's ratio	ν'	0.33
EC model parameter	n_E	1.3

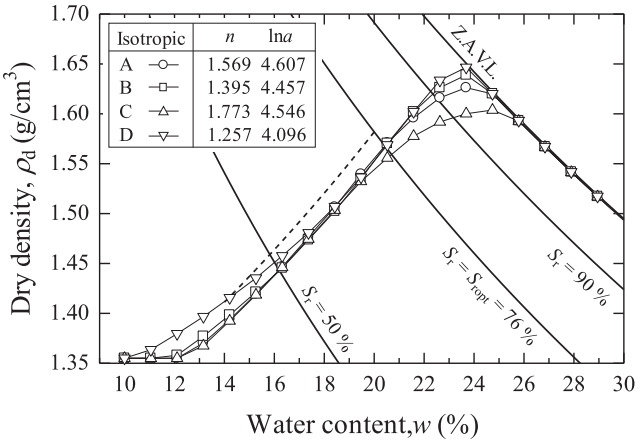

Fig. 14. Results of simulation of static compaction under isotropic condition.

was assumed to be 1.0 on the whole in the above-mentioned calculation. Fig. 15 indicates the possible initial state and the isotropic loading path with a constant water content in addition to both states before and after unloading, as shown in Fig. 3, while subscript α is omitted and so forth. Herein, the initial stress state is assumed to be normally consolidated as well as isotropic. Then, the equation for initial effective mean stress p'_i can be formulated based on Eq. (4), as follows:

$$p'_i = p'_{sat0} \times \xi_i; \quad \xi_i = \xi(S_{e,i}) \tag{31}$$

where term ξ_i can be expressed as a function of initial effective degree of saturation $S_{e,i}$ by Eq. (5) with parameters n and a, while p'_{sat0} denotes the effective mean stress corresponding to the initial void ratio on the NCL for $S_e = 1.0$, as shown in Fig. 15. Hence, we have

$$p'_{sat0} = p'_{sat0}(e_i) = p'_{ref,sat} \exp\left(\frac{e_{ref} - e_i}{\lambda}\right) \tag{32}$$

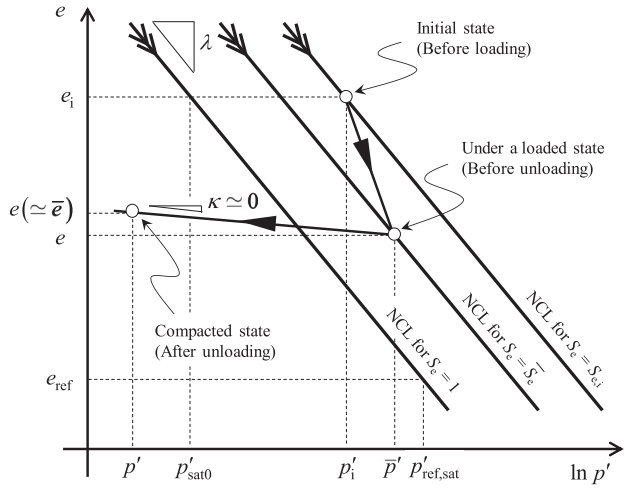

Fig. 15. Possible initial state and isotropic loading path with constant water content.

On the other hand, assuming that the initial state is considered stress-free (zero total stress), initial effective mean stress p'_i can be written in another form based on Eq. (11) as

$$p'_i = S_{e,i}s_i;\ \ s_i = s(S_{e,i}) \tag{33}$$

where initial suction s_i is a function of initial effective degree of saturation $S_{e,i}$ in the inverse form of Eq. (9).

Based on Eqs. (31) and (33), the following condition is obtained for finding a combination of the initial void ratio and the effective degree of saturation:

$$S_{e,i}s(S_{e,i}) - p'_{sat0}(e_i) \times \xi(S_{e,i}) = 0 \tag{34}$$

In fact, a non-linear equation, Eq. (34), can be solved to obtain initial void ratio e_i by imposing constraint $S_{r,i} = wG_s/e_i$ and relation $S_{e,i} = (S_{r,i} - S_{r0})/(1 - S_{r0})$, since the problem in which the water content is given and constant is now being addressed.

The compaction paths with a maximum confining stress of 350 kPa under the constant water content condition, as variations in void ratio with respect to changes in (a) net mean stress, (b) effective mean stress, and (c) degree of saturation, recalculated after the modification of the initial state by solving Eq. (34), are shown by dividing them into the initially dryer states seen in Fig. 16 and the initially wetter ones seen in Fig. 17. Herein, a set of parameters, from the combinations shown in Fig. 13, was used for the calculation (i.e., $n = 1.495$ and $\ln a = 4.457$). In the $e - S_r$ space, the line joining the initial points in the elasto-plastic or normally consolidated state, which can be regarded as an isogram of the net mean stress of 0 kPa, forms a downward convex curve which has a minimal value at much higher degrees of saturation, but declines downward to the right with an increase in the degree of saturation in almost all ranges. Upon loading, each point moves with a decrease in void ratio, maintaining its water content. However, the paths beginning from the wetter and denser states reach the saturated state while loading; thus, the generation of effective mean stress and the decrease in void ratio are terminated, as shown in Fig. 17. On the other hand, for the initially dryer and looser states, shown in Fig. 16, the compression is achieved such that the path extends across the normally consolidated lines of the degree of saturation in the $e - \ln p'$ space until the net mean stress reaches the maximum value of 350 kPa. The line joining the loaded or compacted states has a V-shape in the $e - S_r$ space, whose gradient in a region of the unsaturated state becomes more gentle than that of an isogram of the net mean stress of 0 kPa. While there are some approaches in which the transition of an isogram of the net mean stress upon loading is first formulated to establish the constitutive model for unsaturated soil in previous literatures (e.g., Al-Badran and Schanz, 2009; Yaghoubi et al., 2019), it is of interest that a similar transition can be expressed as the results of the calculation within the approach of this study, so long as the initial states are properly determined in conjunction with the parameters to be input.

The initial and compacted states, obtained as results of the simulation, can be plotted in the $w - \rho_d$ space, as shown in Fig. 18. Herein, the compacted states with the confining stress not only of 350 kPa, but also of 150 and 700 kPa, are provided in order to compare them with the stress isograms, already appearing in Fig. 10, based on the experimental results of the static compaction tests conducted by Kawai et al. (2002). It is found from this figure that the compacted states obtained from the simulations show a good agreement with those from the experimental tests, especially in cases where the maximum confining stress is relatively lower. In cases of higher confining stress levels, lower water contents lead to lower increases estimated in the calculation for the dry density due to compaction. The reasons behind this underestimation might be that the input parameters were estimated based on the

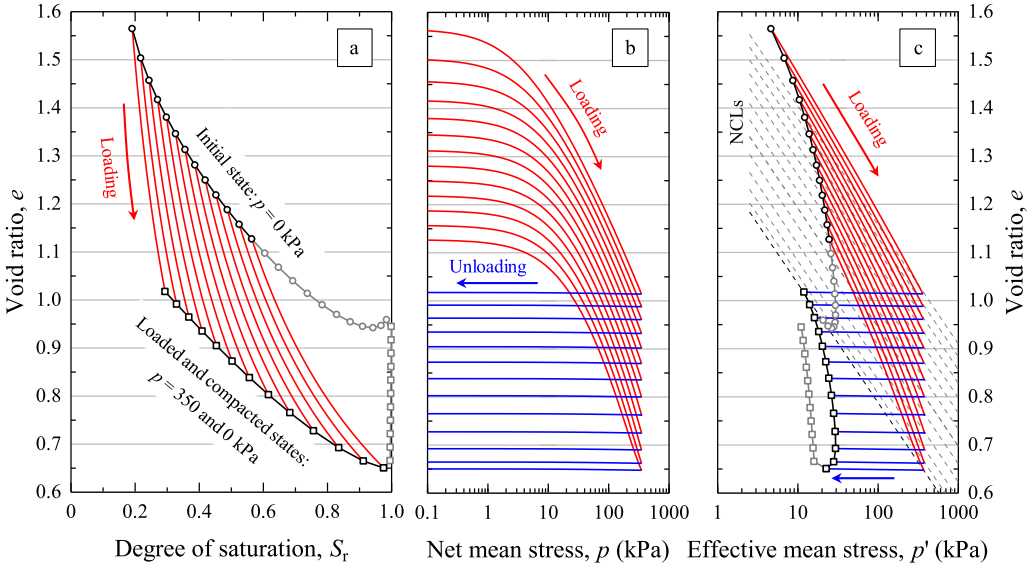

Fig. 16. Recalculated compaction paths for initially dryer states after modification of initial state.

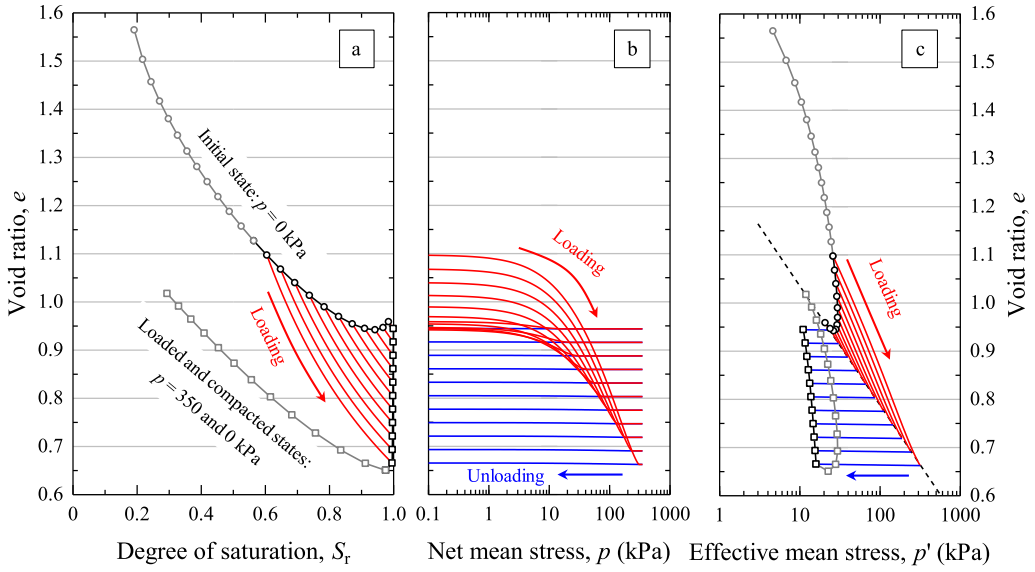

Fig. 17. Recalculated compaction paths for initially wetter states after modification of initial state.

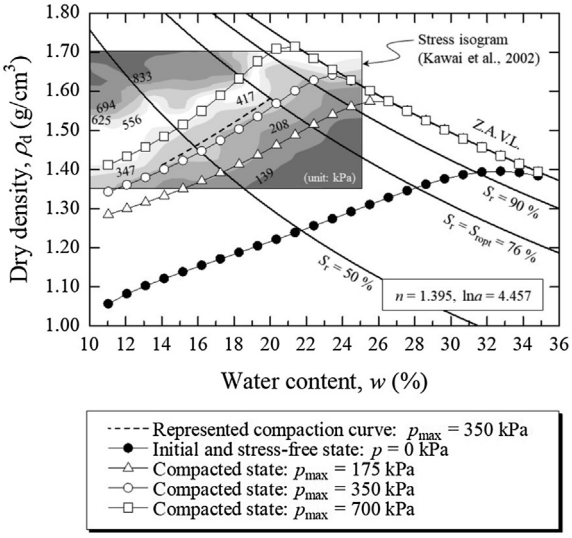

Fig. 18. Initial state and recalculated compaction states with maximum confining stresses of 175, 350, and 350 kPa.

idealized compaction curve of the confining stress of 350 kPa or that there is an inherent limit of the current constitutive model applied in this study in terms of predicting the responses of volume changes due to loading with higher confining stress levels under both wetter and dryer conditions. It would be necessary to reformulate the transition of the normally consolidated line depending upon the degree of saturation, including variations in the compression index, in order to achieve accuracy in predicting the covering of a wider state. Once such a modification is made, the method proposed in this study would be useful for estimating the parameters which are involved in the constitutive model if only a conditional expression, such as Eq. (18), can be formulated for the statically compacted and unsaturated states.

6. Concluding remarks

This paper has presented a method for identifying the parameters for the hardening law of the elasto-plastic constitutive model for unsaturated soils from the compaction curve. The Se-hardening model proposed by Ohno et al. (2007a, 2007b), with two parameters for the hardening law, was employed. The proposed method can be characterized by the following properties:

(1) In the proposed method, two input parameters in the hardening law of the Se-hardening model were estimated by simultaneously solving three theoretical equations, each of which holds for a different point, indicating the statically compacted state on the dry side of the compaction curve.
(2) The dry side of the compaction curve was approximately represented and parameterized using a ternary phase diagram in order to deal with it as a continuous function and to choose three compacted states arbitrarily.
(3) The values of the input parameters estimated with the proposed method hardly depended on the method of sampling the three points on the compaction curve. Although there was a small variation between them, it was found that the parameter variation had only a small influence on the calculated results of the compacted state through a series of simulations of static compaction. This suggests that the parameters can be narrowed even when there are no results from the minute experimental tests accompanied by the control or measurement of the suction.
(4) Once the input parameters are determined, the initial state under a stress-free condition can be theoretically identified for each water content. According to the

simulation of static compaction where such initial states were imposed, the compacted states obtained from the simulations showed a good agreement with those from the experimental tests.

Acknowledgements

The authors gratefully acknowledge Mr. Kazuki Yutaka, a former student of Kobe University, and Mr. Keita Hayashi, a graduate student of Kobe University, for their kind assistance.

References

Al-Badran, Y., Schanz, T., 2009. Yielding surface model of volume change characteristics for unsaturated fine grained soils. In: Buzzi, O., Fityus, S.G., Sheng, D. (Eds.), Unsaturated Soils – Theoretical & Numerical Advances in Unsaturated Soil Mechanics. CRC Press, pp. 863–871.

Alonso, E.E., Gens, A., Josa, A., 1990. A constitutive model for partially saturated soils. Geotechnique 40, 405–435.

Bishop, A.W., 1960. The measurement of pore water pressure in the triaxial test. Proc. Conf. Pore Water Pressure and Suction in Soils. Butterworths, pp. 38–46.

Cui, Y.J., Sun, D.A., 2009. Constitutive modelling: From isothermal to non-isothermal behaviour of unsaturated soils. In: Buzzi, O., Fityus, S. G., Sheng, D. (Eds.), Unsaturated Soils – Theoretical & Numerical Advances in Unsaturated Soil Mechanics. CRC Press, pp. 493–506.

Gens, A., 1996. Constitutive modelling: application to compacted soils. In: Alonso, E.E., Delage, P. (Eds.), Unsaturated Soils, vol. 3, Balkema, Rotterdam, pp. 1179–1200.

Gens, A., Guimaraes, L.do N., Sanchez, M., Sheng, D.C., 2008. Developments in modelling the generalized behavior of unsaturated soils. In: Toll (Ed.), Unsaturated soils: Advances in Geo-Engineering. CRC Press, pp. 53–61.

Iizuka, A., Ohta, H., 1987. A determination procedure of input parameters in elasto-viscoplastic finite element analysis. Soils Found. 27 (3), 71–87.

Kanazawa, S., Toyoshima, T., Kawai, K., Tachibana, S., Iizuka, A., 2012. Analysis of the mechanical behavior of compacted soil with F.E. method. J. JSCE, Division A2: Appl. Mech. 68 (2), 291–298 (in Japanese).

Kawai, K., Kim, E., Nagareta, H., Iizuka, A., Honda, M., 2002. A simple method to predict the consolidation yield stress of compacted soils considering suction effects in unsaturated soil media. J. JSCE, Division A2: Appl. Mech. 5, 785–792 (in Japanese).

Kobayashi, I., 2016. Private communication.

Kohgo, Y., Nakano, M., Miyazaki, T., 1993. Theoretical aspects of constitutive modeling for unsaturated soils. Soils Found. 33 (4), 49–63.

Kohgo, Y., 2003. Review of constitutive models for unsaturated soils and initial boundary value analysis. Proc the 2nd Asian Conference on Unsaturated Soils, pp. 21–40.

Lloret-Cabot, M., Sa´nchez, M., Wheeler, S.J., 2014. Formulation of a three-dimensional constitutive model for unsaturated soils incorporating mechanical-water retention coupling. Int. J. Numer. Anal. Meth. Geomech. 37, 1488–1493.

Lloret-Cabot, M., Wheeler, S.J., Sa´nchez, M., 2017. A unified mechanical and retention model for saturated and unsaturated soil behavior. Acta Geotech. 12, 1–21.

Loret, B., Khalili, N., 2002. An effective stress elasto-plastic model for unsaturated porous media. Mech. Mater. 34, 97–116.

Mikuni, E., 1962. Study on properties of fill dam core material and its compaction No. 1. Monthly Journal of JGS, Tsuchu-to-Kiso, 10(1), 4–12 (in Japanese).

Ohno, S., Kawai, K., Tachibana, S., 2007a. Elasto-plastic constitutive model for unsaturated soil applied effective degree of saturation as a parameter expressing stiffness. J. JSCE, Division C: Geotechnics 63 (4), 1132–1141 (in Japanese).

Ohno, S., Takeyama, T., Pipatpongsa, T., Iizuka, A., Ohta, H., 2007b. Analysis of embankment by nonlinear contractancy description. In: Proc. of the 13th Asian Regional Conference of Soil Mechanics and Geotechnical Engineering, Kolkata, India, pp. 1097–1100.

Ohno, S., Kawai, K., Iizuka, A., Tachibana, S., Kanazawa, S., Ohta, H., 2013. Elasto-plastic constitutive model for unsaturated soils with subloading surface concept. Chapter 14. In: Chu, J., Wardani, Sri P. R., Iizuka, A., (Eds.), Geotechnical Predictions and Practice in Dealing with Geohazards, Geotechnical, Geological and Earthquake Engineering Series, vol. 25, pp. 215–228.

Sheng, D., Fredlund, D.G., 2008. Elastoplastic modelling of unsaturated soils: an overview. In: Proc. of 12th Int. Conf. of International Association for Computer Methods and Advances in Geomechanics, pp. 2084–2105.

Sheng, D., Gens, A., Fredlund, D.C., Sloan, S.W., 2008. Unsaturated soils: from constitutive modelling to numerical algorithms. Comput. Geotech. 35 (6), 810–824.

SoilVision System Ltd., 2006. SoilVision: a knowledge-based database system for unsaturated-saturated soil properties [computer program], Version 4.0. SoilVision System Ltd., Saskatoon, Sask.

Sugii, T., Uno, T., 1995. A new model of soil-water retention characteristics curve. In: Proc. of 50th Annual Meeting of JSCE, pp. 130–131 (in Japanese).

Tatsuoka, F., 2015. Compaction characteristics and physical properties of compacted soil controlled by the degree of saturation. Proc. of 6th International Symposium on Deformation Characteristics of Geomaterials, pp. 40–76.

Wheeler, S.J., Karube, D., 1996. Constitutive modelling. In: Alonso, E.E., Delage, P. (Eds.), Unsaturated soils, vol. 3, Balkema, Rotterdam, pp. 1323–1356.

Wheeler, S.J., Sivakumar, V., 1995. An elasto-plastic critical state framework for unsaturated soil. Int. J. Geotech. 45 (1), 35–53.

Yaghoubi, E., Disfani, M.M., Arulrajah, A., Kodikara, J., 2019. Development of a void ratio-moisture ratio-net stress framework for the prediction of the volumetric behavior of unsaturated granular materials. Soils Found. 59, 443–457.

Zhou, A.N., Sheng, D., Scott, S.W., Gens, A., 2012. Interpretation of unsaturated soil behaviour in the stress-saturation space, I: Volume change and water retention behaviours. Comput. Geotech. 43, 178–187.